Characterization of 167 MeV Xe ion irradiated n-type 4H-SiC

M.J. Madito[a,*], T.T. Hlatshwayo[b], V.A. Skuratov[c,d,e], C.B. Mtshali[a], N. Manyala[b] and Z.M. Khumalo[a]

[a]iThemba LABS, National Research Foundation, PO Box 722, Somerset West 7129, Cape Town, South Africa.

[b]Department of Physics, University of Pretoria, Private Bag X20, Pretoria 0002, South Africa.

[c] FLNR,Joint Institute for Nuclear Research, Dubna, Russia.

[d]National Research Nuclear University MEPhI, Moscow,

[e] Russia Dubna State University, Dubna, Russia

HIGHLIGHTS

• The n-type 4H-SiC with an epitaxial layer was irradiated by 167 MeV Xe ions.

• Three distinct layers of the irradiated sample were demonstrated, including the thicknesses.

• SNOM showed an increase in the optical absorption of the irradiated sample.

ABSTRACT: The nitrogen-doped, n-type 4H-SiC with 6 μm thick epitaxial layer was irradiated at the perpendicular incidence and room temperature by 167 MeV Xe^{+26} ions to a fluence of 5×10^{12} cm^{-2}. The Monte Carlo simulation code, Stopping and Range of Ions in Matter (SRIM) was used to simulate the Xe^{26+} ions irradiated in SiC. The Rutherford backscattering spectrometry (RBS) analysis with 3.5 MeV He^{++} ions which have a projected range of ~9 μm in SiC (SRIM prediction) did not detect implanted Xe. Raman spectroscopy and imaging depth profiles clearly showed three distinct parts of the swift heavy ion (SHI)-irradiated 4H-SiC, i.e. 5.6 μm irradiated epitaxial layer, 6.9 μm damaged irradiated layer and non-irradiated 4H-SiC bulk. Raman spectroscopy showed new broad bands of crystalline Si-Si and distorted Si-C in the damaged irradiated layer. The new Si-Si bands were attributed to the ordering in the Si-Si homonuclear bonds without crystal amorphization. The scanning near-field optical microscopy (SNOM) results of the SHI-irradiated 4H-SiC sample displayed a very low signal counts (transmission) compared to the virgin sample, and this difference in the optical absorption could be correlated with the defects energy levels created within the bandgap of the sample upon irradiation.

KEYWORDS: 4H-SiC; SNOM; Depth profiles; Xe ions; Silicon carbide; Epitaxial layer

Corresponding authors email addresses:
*mmadito@tlabs.ac.za (M.J. Madito)

1. INTRODUCTION

The device developments in the nuclear energy environment require radiation-resistant electronic materials. Silicon carbide (SiC), with typical applications in the fields of electronic power devices, is stable under high-temperature and radiation environments (e.g. high-temperature reactor (HRT)) owing to its structural, chemical and mechanical stability [1]. However, for the application of SiC in new advanced radiation-hard electronic devices, in-depth knowledge of its response (and characterization) to radiation damage is required for refined control purposes. Studies have been carried out to create harsh radiation conditions from swift heavy ions (SHI) in SiC, and have shown that the structure strongly changes with increasing radiation fluence [2–4]. The SHI irradiation of SiC could degrade or enhance the performance of the crystal in certain applications. For instance, a 4H-SiC ultraviolet photodetector irradiated with 167 MeV Xe ions has retained its performance with enhanced service life and radiation endurance at elevated temperatures [5].

To date, studies have been done on amorphization [4,6–10], annealing processes [11–13] and recrystallization [4,14–17] of ion irradiated SiC. However, in most studies, a large area characterization of the SHI-irradiated depth/region is in general limited due to the exclusive use of the Rutherford backscattering spectrometry (RBS) ion-channeling method and high-resolution transmission electron microscopy (HRTEM) technique. In this regard, the Monte Carlo simulation code, Stopping and Range of Ions in Matter (SRIM) have been used to simulate the projected range of the swift heavy ions in SiC, including the damage induced by elastic knock-on processes and recoiling nuclei in the electronic slowing-down regime. Sorieul *et al*. [10] have demonstrated a large area characterization (z-scan depth of 5 μm) of the SHI-irradiated α-SiC with a spectroscopic technique, namely, Raman spectroscopy which is less destructive and provides structural information of the sample including the transformation between the crystalline and amorphous state of the sample, and chemical reordering (the formation of homonuclear bonds) in irradiated SiC. In the study by Sorieul *et al*., the confocal depth resolution of the Raman system used was 7 μm (measured from the virgin 6H-SiC sample). Therefore, the Raman spectra of irradiated SiC acquired within a z-scan depth of 5 μm composed of contributions from the irradiated layer and the non-irradiated part of the sample. Contrary to their study, the confocal depth resolution of the Raman system we used in our study is 2.4 μm and this was obtained from the measured Raman depth profile of the virgin 4H-SiC sample with an epitaxial layer of a known thickness. Also, for better accuracy, the contributions of other parts in the Raman spectrum

were subtracted using the "true component analysis demixing of spectra" (data processing tool of a WITec Project FIVE software) and the standard spectra from the virgin sample.

Herein we report on the SRIM simulation and characterization of SHI-irradiated nitrogen-doped, n-type 4H-SiC by RBS, Raman spectroscopy and imaging depth profiles, and scanning near-field optical microscopy (SNOM) coupled with atomic force microscopy (AFM) imaging. We demonstrate three distinct parts of the irradiated sample (i.e. irradiated epitaxial layer, damaged irradiated layer and non-irradiated 4H-SiC bulk) and the thicknesses of the layers including the chemical compositions. Furthermore, the SNOM data showed an increase in the optical absorption of the irradiated sample, as expected, since radiation-induced point defects could create defects energy levels within the bandgap of the material altering the optical absorption.

2. EXPERIMENTAL

Nitrogen-doped, n-type (0001) oriented 4H-SiC (8° off-axis) wafers from CREE Research Inc. were used in this work. The wafer consists of a 6 μm thick epitaxial layer with nitrogen doping density of 6×10^{16} cm^{-3} grown by chemical vapour deposition on the highly doped SiC substrate with a doping density of $\sim 10^{18}$ cm^{-3}. The samples were irradiated at the perpendicular incidence and room temperature by 167 MeV Xe^{+26} ions to a fluence of 5×10^{12} cm^{-2}. During the irradiation, the beam was raster scanned. The irradiation was carried out at the Joint Institute of Nuclear Research in Dubna, Russia using the IC-100 FLNR cyclotron. SRIM was used to simulate the Xe^{26+} ions in 4H-SiC. In SRIM calculations, an option ''Detailed Calculation with full Damage Cascades'' which follows every recoil until its energy drops below the lowest displacement energy of a target atom, was used to compute the ion-induced displacement damage parameters. The calculations were carried out using the SRIM-2013 version, the threshold displacement energies of 20 and 35 eV for the C and Si sublattices respectively were used [18], with the lattice binding energies set to zero [19]. Incident ions of 10 000 were used to improve statistics. The SRIM vacancies/ion number was converted into displacements per atom (dpa) as follows:

$$dpa = \frac{\left(Vacancies / ion \cdot \overset{0}{\text{A}} \right) \times 10^{8}}{N_a} \times \phi \qquad (1)$$

where ϕ (ions/cm^2) is the ion fluence, N_a is the atomic density ($N_a = 9.64 \times 10^{22}$ atoms/cm^3 for SiC), and 10^8 is the conversion factor from angstrom to a centimetre.

Rutherford backscattering spectrometry analysis of both virgin and irradiated samples were performed at room temperature and vacuum pressure better than 10^{-6} mbar using a 3.5 MeV beam of He^{++} ions at a scattering angle of 150^0 using Si surface barrier detector with an energy resolution of about 23 keV. A total charge of 20 μC was collected per measurement to improve statistics. Average current of 40 nA was used throughout measurements.

WITec alpha300 RAS+ confocal Raman microscope was used for cross-sectional depth profile imaging of the virgin and SHI-irradiated 4H-SiC samples. The analysis was carried out using a 100×/0.9NA objective and 532 nm laser at a power of 5 mW. The Raman *z*-scan (depth) images were acquired over width and depth of 70 μm with 200 points per line and 200 lines per image using an integration time of 0.5 s. The image scans were obtained by scanning the sample under the laser spot using a piezo-scanner which is quite fast and very accurate. The diffraction-limited laser spot size is estimated by $\Delta x = 0.61 \times \lambda / NA$, where λ is the wavelength and *NA* is the numerical aperture of the objective used for analysis. Therefore, for 100×/0.9*NA* objective used in this work, the lateral resolution is about 361 nm. The spectral resolution is in the order of 1 cm^{-1}. The confocal depth resolution was obtained as 2.4 μm from the Raman depth profile of the virgin 4H-SiC sample with a 6 μm thick epitaxial layer. WITec project five software version was used for data processing. For SNOM imaging in transmission, a 60×/0.8*NA* objective, and 532 nm laser at a power of 3 mW was used. The SNOM cantilever was used for concurrent SNOM and AFM imaging in contact mode. A switch between the Raman and SNOM modes was achieved by rotating the microscope turret without moving the position of the sample.

3. RESULTS AND DISCUSSION

Figure 1 displays a schematic illustration of the SHI-irradiated n-type 4H-SiC with 6 μm thick epitaxial layer (figure 1(a)) together with SRIM simulations (figure 1(b)-(e)). Figure 1(b) shows trajectories of 167 MeV Xe ions into SiC bulk and the projected range, R_p. The subcascades generated by recoiling lattice atoms are distributed along the trajectory lines of the Xe ions. As the number of incident ions on the target increases, the irradiation trajectories begin to overlap and more uniform distribution of subcascade damage is imparted to the target material at the projected range, but only if the ion fluence is sufficient to cause damage.

Figure 1(c) shows the number of target-atom vacancies per ion per nanometer along the path of the Xe ions and the corresponding ion distributions with nearly Gaussian profile at the mean range of R_p = 12.9 μm. The statistical value of target-atom vacancy per ion averaged over 40865. Figure 1(d) shows the displacements per atom and the displaced atoms distributions along the path of the Xe ions as they come to rest in SiC bulk. Typically, the dpa is the statistical average of the fractional number of lattice atoms which have been displaced. Accordingly, in the projected range of 167 MeV Xe ions in SiC (i.e. in the damaged irradiated layer) the maximum dpa is 0.0081 now, on average, 0.81% of the target atoms experienced displacement. In the irradiated epitaxial layer, the maximum dpa is 0.00065 then, on average, 0.065% of the target atoms experienced displacement. Based on this, it can be suggested that an insignificant fraction of atoms in the irradiated epitaxial layer experienced lattice displacement and only about 1% were displaced in the damaged irradiated layer and did not result in amorphization. It is worth noting that these calculations give the mean damage distribution for ions with the same initial conditions. Sorieul *et al*. [10] have shown that for the lowest dpa of 0.003, the Raman spectrum of the SHI-irradiated α-SiC sample is similar to the virgin one, which suggests that α-SiC is weakly damaged or undamaged. Sorieul *et al*. have also shown that for amorphization of α-SiC, a minimum of 0.264 dpa is required. Furthermore, as 167 MeV Xe ions impinge 4H-SiC bulk, they lose energy via electronic and nuclear collision processes (Figure 1(e)) until they come to rest. The latter process is responsible for radiation-damage effects in the crystal. From figure 1(e), the maximum electronic and nuclear energy loss values are 20.4 and 1.3 keV/nm, respectively. These values are less than the threshold ionizing radiation level, i.e. lower than the electronic stopping power (Se = 34 keV/nm [20,21]) for the formation of amorphous tracks in SiC, hence Xe ions did not form tracks during irradiation. Briefly, the SRIM calculations show that the irradiated epitaxial layer and the damaged irradiated layer mainly experienced electron energy loss and nuclear energy loss respectively. The latter energy loss induced isolated vacancy-interstitial defects (Frenkel-defects) in the damaged irradiated layer but did not result in amorphization, and the electron energy loss induced electrically active defects (both point defects and complexes) mainly in the irradiated epitaxial layer [22].

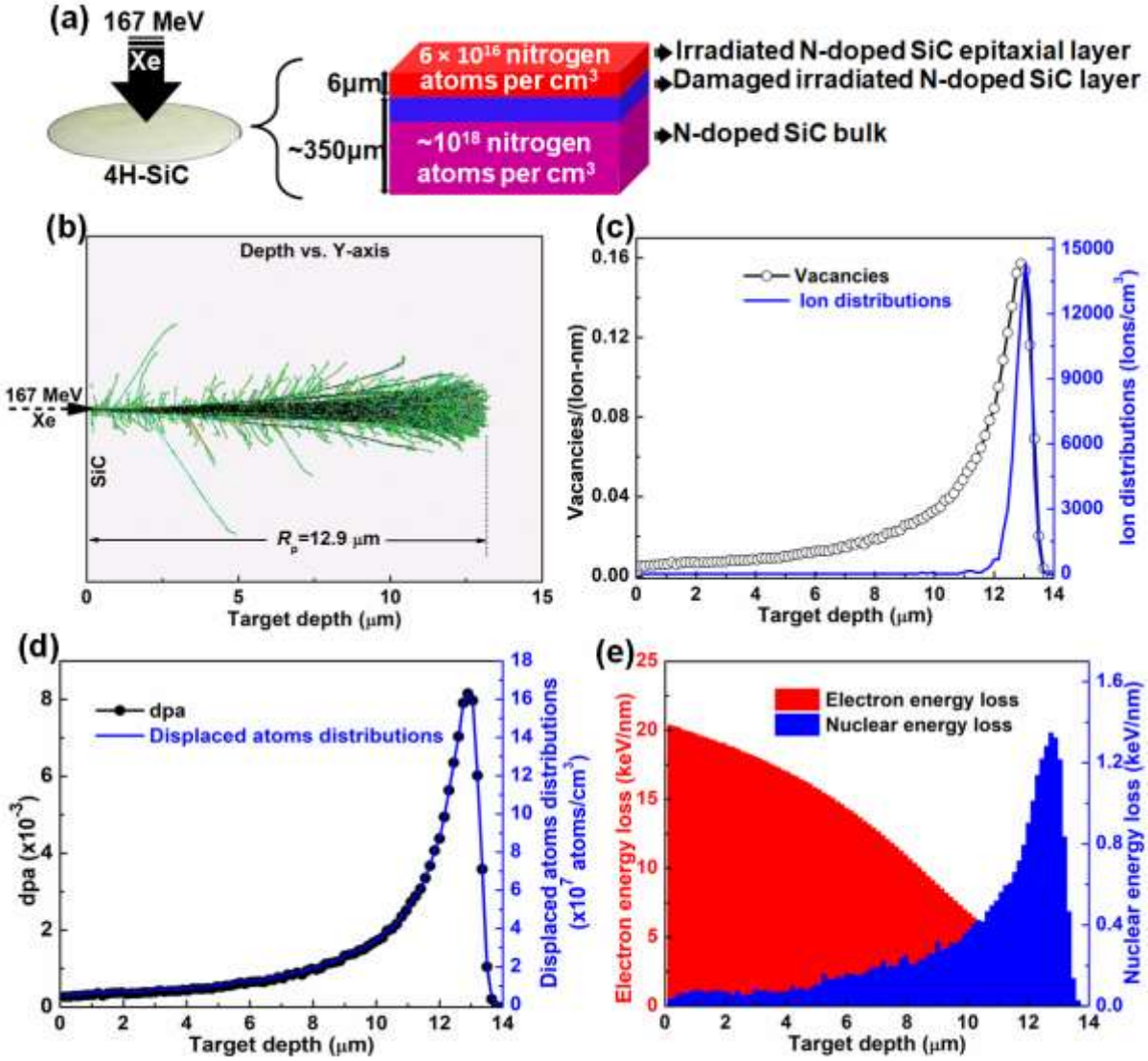

Figure 1. (a) Schematic illustration of the SHI-irradiated 4H-SiC with ~6 µm thick epitaxial layer. SRIM calculations of 167 MeV Xe ions in 4H-SiC: (b) Trajectories of Xe ions into 4H-SiC bulk. (c) Vacancy and ion distribution profiles. (d) The displacements per atom (dpa) and displaced atoms distributions profiles. (e) The electron and nuclear energy loss with depth.

The measured RBS spectra for 3.5 MeV He^{++} ions backscattered from virgin and SHI-irradiated 4H-SiC samples are shown in figure 2, as well as the simulated backscattering spectrum of the irradiated sample. The simulated spectrum was obtained using SIMNRA software version 7.02 [www.simnra.com]. In figure 2, there is no noticeable peak from the Xe located in the damaged irradiated layer at the projected range of 12.9 µm, predominantly because this is beyond the projected range of the 3.5 MeV He^{+} ions in SiC which is ~9 µm (SRIM prediction), and this could also be due to low radiation fluence used.

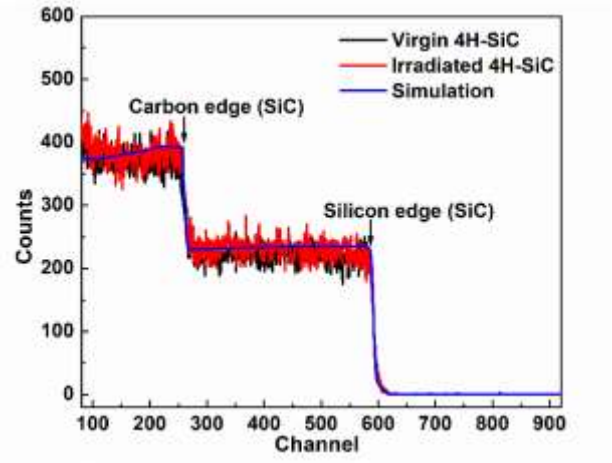

Figure 2. RBS spectra of the virgin and SHI-irradiated 4H-SiC samples, and the simulated spectrum of the irradiated sample.

Figure 3(a) shows a characteristic Raman spectrum of 4H-SiC bulk. From this figure, the A_1(LO), E_1(TO) and E_2 phonon modes are observed as expected to be seen in the Raman spectrum of 4H-SiC. The group theory has shown that the Raman-active modes of the wurtzite structure (C6v symmetry for hexagonal polytypes) are the A_1, E_1 and E_2 modes; the A_1 and E_1 modes split into longitudinal (LO) and transverse (TO) optical modes, respectively [2,20,23,24]. Figure 3(b) shows the Raman spectra of the irradiated 4H-SiC sample. These spectra were obtained from the crystal surface for epitaxial layer and from the *z*-scan depth of 12 and 20 μm for the damaged irradiated layer and non-irradiated 4H-SiC bulk respectively. In figure 3(b), it can be seen that the main regions of the Si-Si bands (~100 – 600 cm^{-1}), as well as the Si-C bands (~700 – 1000 cm^{-1}), differ in that the new broad bands appear upon irradiation, as shown with Lorentzian fit in figure 3(c). The bands from the Lorentzian fit and the corresponding assignments identified from previous studies are listed in table 1. The new Si-Si bands upon irradiation might be attributed to the ordering in the Si-Si homonuclear bonds without crystal amorphization. This suggests the growth of Si-Si nanocrystallites in the damaged irradiated layer through the distortion of Si-C network since the Si-C bands appearing upon irradiation (Figure 3(c)) might be attributed to the distorted Si-C network by ion irradiation (see table 1). Typically the A_1(LO) phonon mode in 4H-SiC shows a direct dependency on the carrier concentration [25]. After SHI irradiation, the A_1(LO) peak of a 4H-SiC bulk at 976.7 cm^{-1} is narrowed (its intensity is higher) and shifted to a lower wavenumber of 964.9 cm^{-1} (see insert to figure 3(b) and table 2). A similar A_1(LO) peak behavior was seen

in Ref. [25] from the Raman spectra of the 4H-SiC bulk with high n-type doping concentration compared to the one with low doping concentration. Therefore, SHI irradiation reduces the interaction of free carriers (from n-type doping) with LO phonons in the damaged irradiated layer since a narrow peak at about 964 cm^{-1} is assigned to the LO mode without coupling and that at ~980 cm^{-1} arises from longitudinal optical phonon-plasmon coupling mode originating from the interaction of free carriers with LO phonons [23–26]. The epitaxial layer of both the unirradiated and irradiated sample show similar Raman spectra (Figure 3(d)), however, with a slight decrease in A_1(LO)-to-E_2(TO) peak ratio and this suggests that the epitaxial layer was slightly or not affected by the SHI irradiation, the nuclear energy loss process in particular, as shown by SRIM calculations.

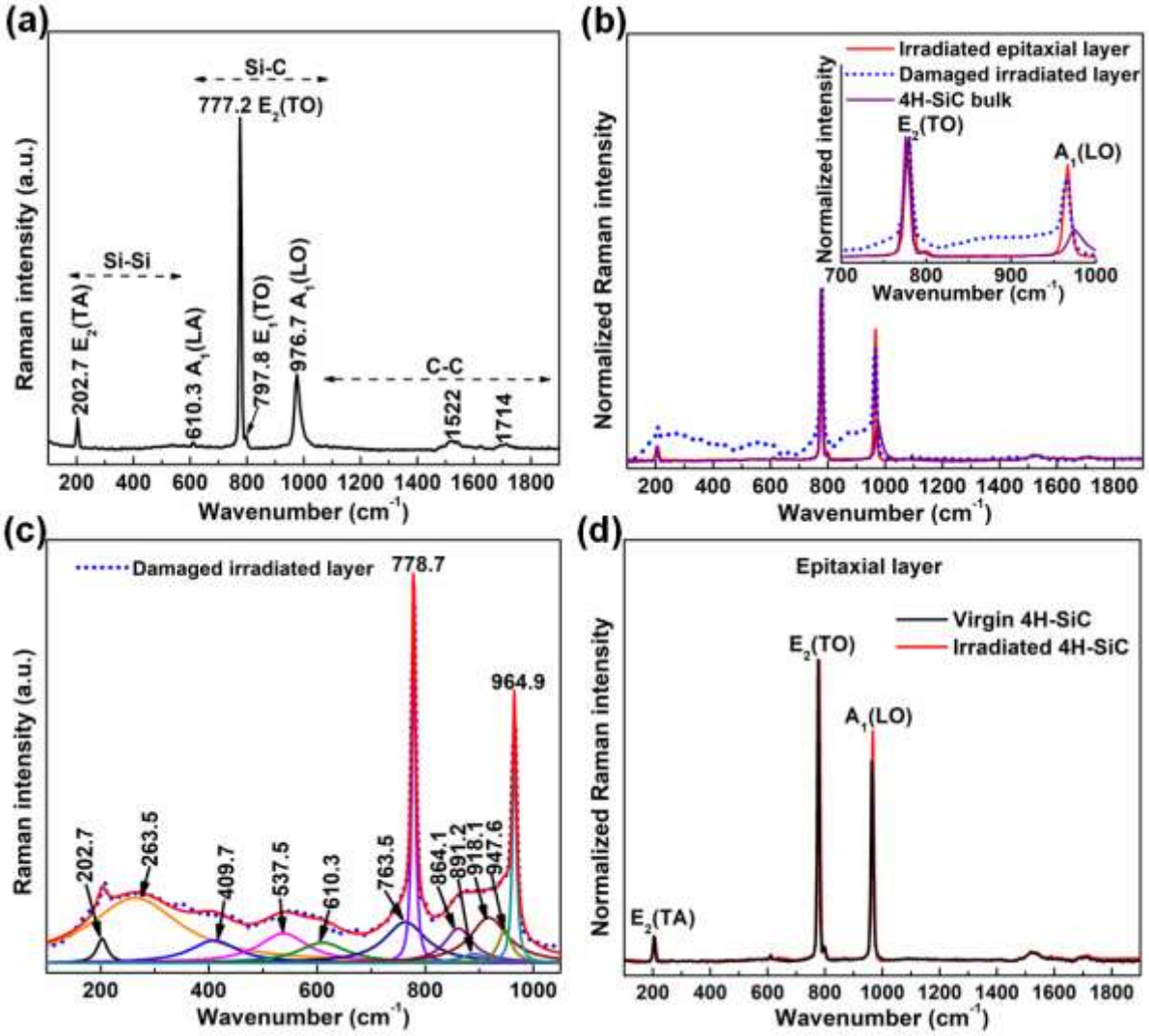

Figure 3. Raman spectra: (a) 4H-SiC bulk, (b) SHI-irradiated 4H-SiC, (c) Lorentzian fit of the spectrum of the damaged bulk region in (b), and (d) the unirradiated and irradiated epitaxial layer of the 4H-SiC. In (b) and (d) the spectra are normalized to the E_2(TO) peak.

Table 1. The bands from the Lorentzian fit in figure 3(c) and the corresponding assignments identified from previous studies. The shaded rows show the new bands upon irradiation in the damaged irradiated layer.

Bands (cm^{-1})	Bonds	Local structure	Phonon modes	Ref.
202.7	Si-Si	Crystalline	E_2(TA)	[25][24]
263.5	Si-Si	Crystalline	E_1(TA)	[25][24]
409.7	Si-Si	Crystalline	E_2(TO)	[10]
537.9	Si-Si	Crystalline	E_2(TO)	[25][24]
610.3	Si-C	Slightly distorted	A_1(LA)	[10]
763.5	Si-C	Crystalline	E_2(TO)	[25][24]
778.7	Si-C	Crystalline	E_2(TO)	[25][24]
864.1	Si-C	Highly disordered	-	[10]
891.2	Si-C	Highly disordered	-	[10]
918.1	Si-C	Slightly disordered	-	[10]
947.6	Si-C	Slightly disordered	-	[10]
964.9	Si-C	Slightly distorted (N-Doping in the crystal)	A_1(LO)	[10][25][24]

Table 2. The E_2(TO) and A_1(LO) peak positions, full width at half maximum (FWHM) and the A_1(LO)-to-E_2(TO) peak ratio for the unirradiated and irradiated 4H-SiC.

	Epitaxial layer					**4H-SiC bulk**				
	E_2(TO) mode		**A_1(LO) mode**			**E_2(TO) mode**		**A_1(LO) mode**		
	Position (cm^{-1})	FWHM (cm^{-1})	Position (cm^{-1})	FWHM (cm^{-1})	**A_1(LO)/ E_2(TO)**	Position (cm^{-1})	FWHM (cm^{-1})	Position (cm^{-1})	FWHM (cm^{-1})	**A_1(LO)/ E_2(TO)**
Unirradiated	777.3	6.5	964.5	6.6	0.74	777.2	6.5	976.7	21.7	0.22
Irradiated	778.7	7.0	964.9	8.1	0.66	778.7	8.5	964.9	9.0	0.66

Figure 4 shows the Raman imaging depth profiles of the SHI-irradiated 4H-SiC sample. The depth profiles were used to estimate the thickness of the irradiated epitaxial and damaged irradiated layer. Figure 4(a) and 4(b) shows the Raman mapping of the A_1(LO) peak positions and FWHMs respectively, for the irradiated 4H-SiC sample. These depth profiles display a uniform map with two distinct parts. The first top part (0 – 13 μm) consists of the irradiated epitaxial and damaged irradiated layer and the second part is the non-irradiated 4H-SiC bulk (>13 μm). From these depth profiles, it can be seen that the projected range of irradiation is about 13 μm in agreement with SRIM calculations; however, with these profiles the irradiated epitaxial and damaged irradiated layer are not distinguishable. To distinguish the two layers, the true component analysis was carried out, as shown in figure 4(c) to 4(e). Briefly, from the spectral data set the true component analysis finds components automatically, creates intensity distribution images (component mapping) with corresponding

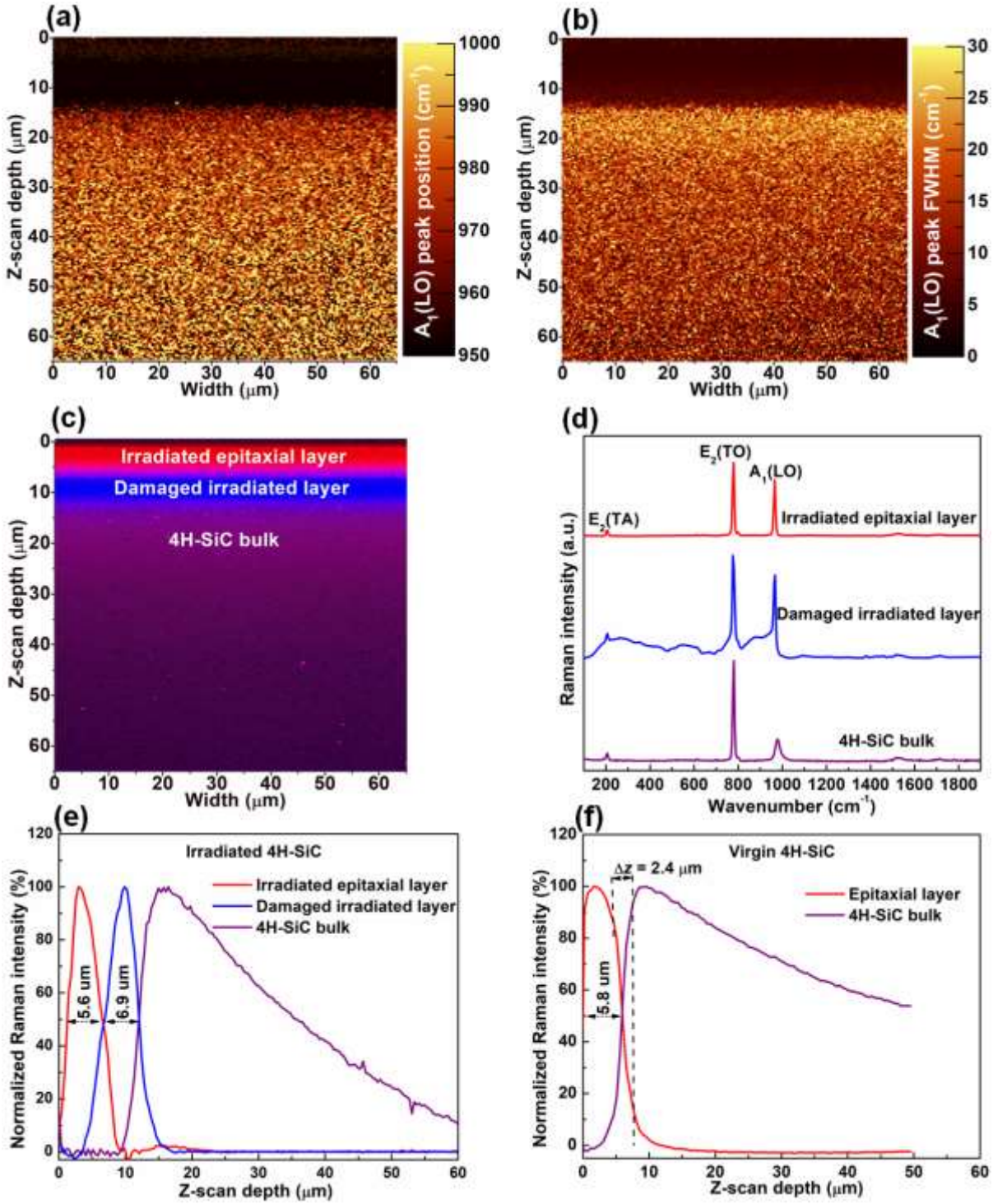

Figure 4. Raman imaging depth profiles of the SHI-irradiated 4H-SiC sample: (a) and (b) A_1(LO) peak positions and FWHMs, respectively. (c) and (d) True component mapping and corresponding components average spectra, respectively. (e) True component depth profile (average intensity plot of true component mapping in (c)) of the SHI-irradiated 4H-SiC sample. (f) True component depth profile of the virgin 4H-SiC sample.

average component spectra that show the distribution of different components and supports demixing of spectra. The true component analysis clearly shows three distinct parts of the irradiated sample, i.e. irradiated epitaxial layer, damaged irradiated layer and non-irradiated 4H-SiC bulk, as shown by component mapping in figure 4(c) and the corresponding average component spectra in figure 4(d). The spectra in figure 4(d) are similar to those discussed in figure 3(b). At 50% of the maximum Raman intensity (Figure 4(e)) the irradiated epitaxial layer has a thickness of 5.6 μm and the damaged irradiated layer of 6.9 μm. In addition, the damaged irradiated layer has a maximum depth of 12.5 μm corresponding to the SRIM projected range; however, beyond the irradiated layer there is a drastic reduction in the Raman intensity from deeper depth which could be attributed to the increase in optical absorption (at a photon energy of ~2.5 eV) in the damaged irradiated layer of the material [20]. To further analyse the optical absorption of the SHI-irradiated sample, the optical imaging was obtained using the SNOM coupled with AFM. Moreover, the confocal Raman depth resolution (Δz) of 2.4 μm was obtained from the depth profile of the virgin 4H-SiC sample, as shown in figure 4(f). This depth profile was acquired using the same system settings used for the irradiated sample. The depth resolution, Δz = 2.4 μm corresponds to the depth range over which an 84 to 16% change in the full signal of the epitaxial layer was measured.

In SNOM, an optical image is obtained by scanning a sample at a small distance (near-field, ~6 nm) below the aperture with a diameter smaller (<100 nm) than the excitation wavelength (see schematic illustration in figure 5(a)). In this setup, the optical resolution of the transmitted light is only limited by the diameter of the aperture. The SNOM cantilever is used for obtaining both optical and topographical (AFM) images concurrently. Figure 5(b) to 5(d) show the SNOM results for virgin and SHI-irradiated 4H-SiC samples which display a noticeable difference in the optical absorption of the two samples. The irradiated sample shows very low signal counts (transmission) compared to the virgin sample. This reduction in signal transmission upon SHI irradiation could be correlated with the defects energy levels created within the bandgap of the sample due to radiation-induced point defects [20,27,28]. From the near-field optical images (Figure 5(c) and 5(d)) as well as the signal cross-section line profiles (Figure 5(b)) obtained along the lines shown in these images, it can be seen that the samples have grooves nanostructure. These nanostructured patterns of the samples can properly be seen from the AFM images (Figure 6(a) and 6(b)) obtained from the back of the sample (opposite epitaxial layer). Therefore, the groove patterns observed in the SNOM data

are mainly due to the surface roughness of the sample, as shown by AFM data. In addition, the epitaxial layer of both the virgin and SHI-irradiated 4H-SiC samples show similar surface roughness, ~1 nm (Figure 6(c) and 6(d)), and this further suggests that the surface of the epitaxial layer was slightly or not modified by the SHI irradiation.

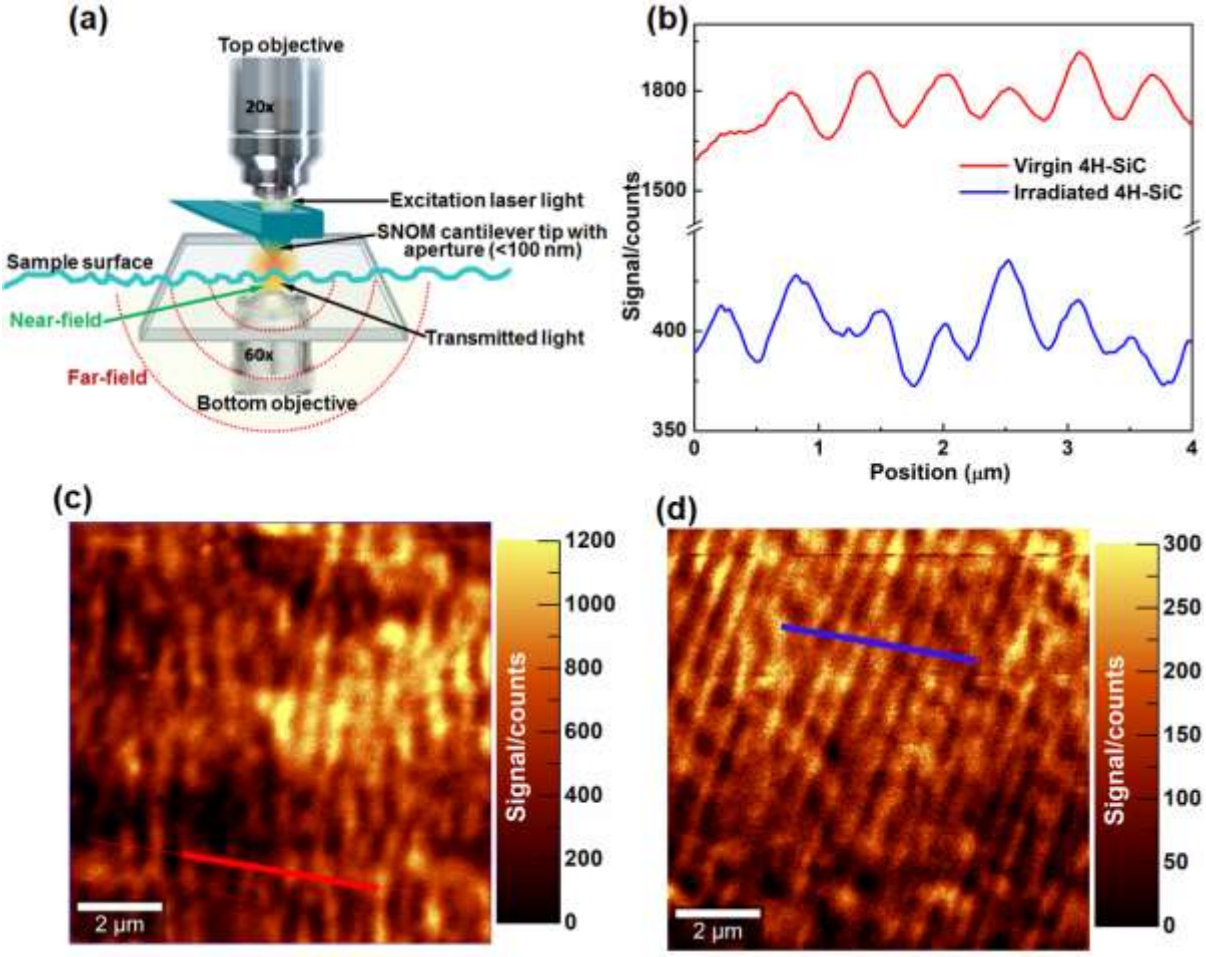

Figure 5. (a) Schematic illustration of the SNOM setup. SNOM results for virgin and SHI-irradiated 4H-SiC samples: (b) The signal cross-section line profiles obtained along the lines shown in (c) and (d). (c) and (d) Near-field optical images for virgin and irradiated samples, respectively.

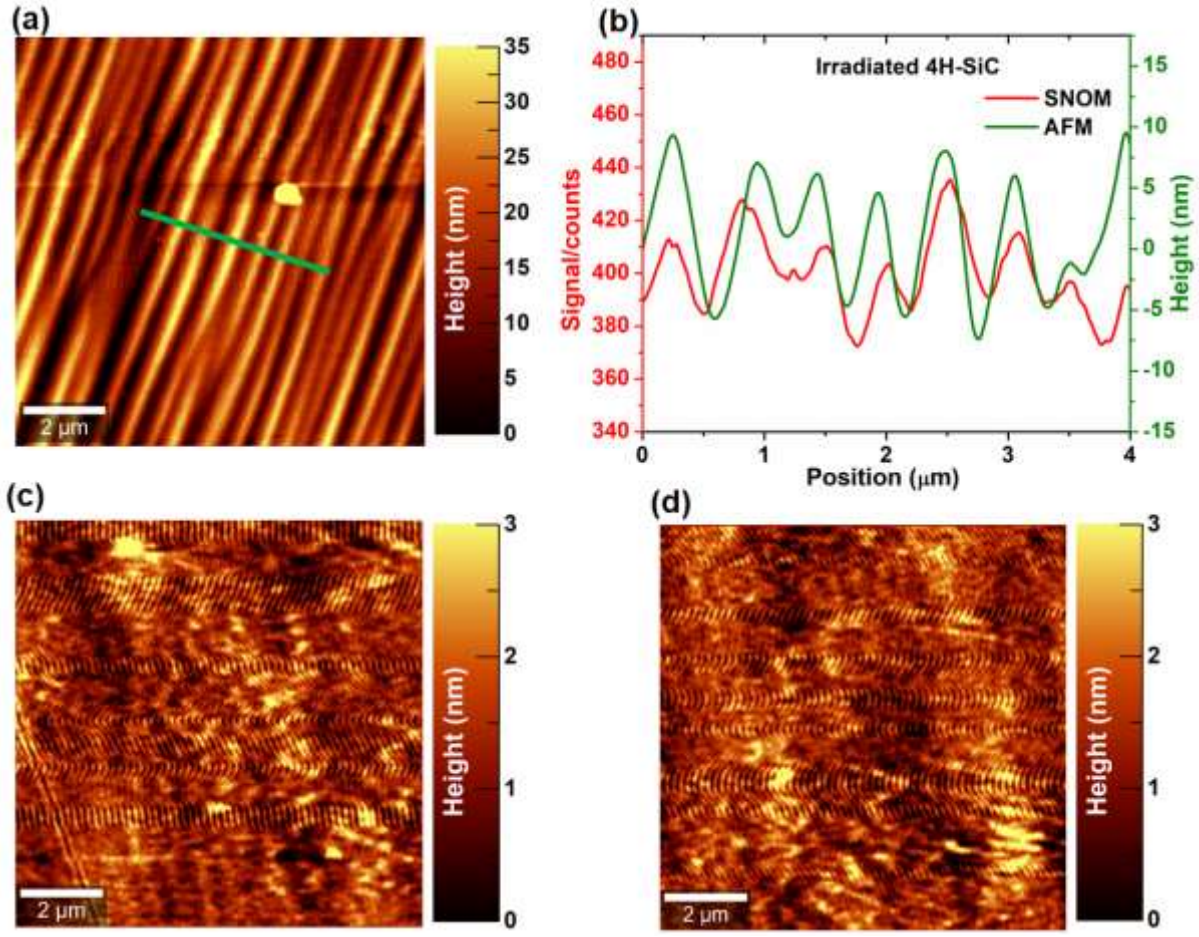

Figure 6. AFM images: (a) From the back of the 4H-SiC sample (opposite epitaxial layer). (b) The signal cross-section line profiles obtained along the lines shown in (a) and figure 5. (c) and (d) The surface of the epitaxial layer of the virgin and SHI-irradiated 4H-SiC sample, respectively.

4. CONCLUSION

In this study, the nitrogen-doped, n-type (0001) oriented 4H-SiC with 6 µm epitaxial layer was irradiated at the perpendicular incidence and room temperature by 167 MeV Xe^{+26} ions to a fluence of 5×10^{12} cm^{-2}. The SRIM calculations were used to simulate the Xe^{26+} ions in SiC, and the characterization was carried out by RBS, Raman spectroscopy and imaging depth profiles, and SNOM coupled with AFM imaging. Based on SRIM simulations, an insignificant fraction (<0.1%) of atoms in the irradiated epitaxial layer of the 4H-SiC experienced lattice displacement and only about 1% in the damaged irradiated layer and SHI irradiation did not result in amorphization of the crystal. The RBS analysis with 3.5 MeV He^{++} ions which have a projected range of ~9 µm in SiC (SRIM prediction) does not show Xe located in the damaged irradiated layer. This could be due to low radiation fluence used and

the projected range (>9 μm) of Xe^{26+} ions in 4H-SiC. Raman spectroscopy and imaging depth profiles clearly showed three distinct parts of the SHI-irradiated 4H-SiC sample, i.e. irradiated epitaxial layer, damaged irradiated layer and non-irradiated 4H-SiC bulk. The irradiated epitaxial layer displayed a thickness of 5.6 μm and the damaged irradiated layer of 6.9 μm. Besides, the damaged irradiated layer displayed a maximum depth of 12.5 μm corresponding to the SRIM projected range. Moreover, the Raman spectroscopy showed new broad bands (crystalline Si-Si and distorted Si-C) in the damaged irradiated layer and the Si-Si bands might be attributed to the ordering in the Si-Si homonuclear bonds. This suggests the growth of Si-Si nanocrystallites in the damaged irradiated layer through the distortion of Si-C network. After SHI irradiation, the A_1(LO) peak of a 4H-SiC bulk at 976.7 cm^{-1} which arises from longitudinal optical phonon-plasmon coupling mode originating from the interaction of free carriers with LO phonons increased in intensity and shifted to 964.9 cm^{-1} mode which is assigned to the LO mode without coupling. A similar A_1(LO) peak behavior was seen by Burton *et al*. [25] from the Raman spectra of the 4H-SiC bulk with high n-type doping concentration compared to the one with low doping concentration. Therefore, SHI irradiation reduces the interaction of free carriers (from n-type doping) with LO phonons in the damaged irradiated layer. The SNOM results of the SHI-irradiated 4H-SiC sample displayed a very low signal counts (transmission) compared to virgin sample, as expected and this difference in the optical absorption could be correlated with the defects energy levels created within the bandgap of the sample upon irradiation. The epitaxial layer of both the virgin and SHI-irradiated 4H-SiC sample showed similar surface roughness. Future work will focus on the characterization of a trilayer α-SiC samples (i.e. irradiated epitaxial layer, amorphous interlayer and damaged irradiated layer without amorphization) fabricated by SHI and slow ions irradiation.

ACKNOWLEDGEMENTS

This work is based on the research supported by the National Research Foundation of South Africa (NRF) via iThemba LABS Materials Research Department (MRD). The author would like to thank ion beam analysis (IBA) group, software developers, and Tandetron operators for their assistance.

REFERENCES:

[1] A.T. Paradzah, F.D. Auret, M.J. Legodi, E. Omotoso, M. Diale, Electrical characterization of 5.4 MeV alpha-particle irradiated 4H-SiC with low doping density, Nucl. Instruments Methods Phys. Res. Sect. B Beam Interact. with Mater. Atoms. 358 (2015) 112–116. doi:10.1016/J.NIMB.2015.06.006.

[2] S. Sorieul, J.-M. Costantini, L. Gosmain, L. Thomé, J.-J. Grob, Raman spectroscopy study of heavy-ion-irradiated α-SiC, J. Phys. Condens. Matter. 18 (2006) 5235–5251. doi:10.1088/0953-8984/18/22/022.

[3] J.B. Hlatshwayo, T.T.; O'Connell, J.H.; Skuratov, V.A.; Wendler, E.; Njoroga, E.G.; Mlambo, M.; Malherbe, Comparative study of the effect of swift heavy ion irradiation at 500 °C and annealing at 500 °C on implanted silicon carbide, (2016) 68593–68598.

[4] T.T. Hlatshwayo, J.H. O'Connell, V.A. Skuratov, M. Msimanga, R.J. Kuhudzai, E.G. Njoroge, J.B. Malherbe, Effect of Xe ion (167 MeV) irradiation on polycrystalline SiC implanted with Kr and Xe at room temperature, J. Phys. D. Appl. Phys. 48 (2015) 465306. doi:10.1088/0022-3727/48/46/465306.

[5] E. V. Kalinina, A.A. Lebedev, E. Bogdanova, B. Berenquier, L. Ottaviani, G.N. Violina, V.A. Skuratov, Irradiation of 4H-SiC UV detectors with heavy ions, Semiconductors. 49 (2015) 540–546. doi:10.1134/S1063782615040132.

[6] L.L. Snead, S.J. Zinkle, Amorphization and the Effect of Implanted Ions in SiC, MRS Proc. 373 (1994) 377. doi:10.1557/PROC-373-377.

[7] S.J. Zinkle, L.L. Snead, Influence of irradiation spectrum and implanted ions on the amorphization of ceramics, Nucl. Instruments Methods Phys. Res. Sect. B Beam Interact. with Mater. Atoms. 116 (1996) 92–101. doi:10.1016/0168-583X(96)00016-X.

[8] W.J. Weber, L.M. Wang, N. Yu, N.J. Hess, Structure and properties of ion-beam-modified (6H) silicon carbide, Mater. Sci. Eng. A. 253 (1998) 62–70. doi:10.1016/S0921-5093(98)00710-2.

[9] E. Wendler, A. Heft, W. Wesch, Ion-beam induced damage and annealing behaviour in SiC, Nucl. Instruments Methods Phys. Res. Sect. B Beam Interact. with Mater. Atoms. 141 (1998) 105–117. doi:10.1016/S0168-583X(98)00083-4.

[10] S. Sorieul, J.M. Costantini, L. Gosmain, L. Thomé, J.J. Grob, Raman spectroscopy study of heavy-ion-irradiated α-SiC, J. Phys. Condens. Matter. 18 (2006) 5235–5251.

doi:10.1088/0953-8984/18/22/022.

[11] J. Grisolia, B. de Mauduit, J. Gimbert, T. Billon, G. Ben Assayag, C. Bourgerette, A. Claverie, TEM studies of the defects introduced by ion implantation in SiC, Nucl. Instruments Methods Phys. Res. Sect. B Beam Interact. with Mater. Atoms. 147 (1999) 62–67. doi:10.1016/S0168-583X(98)00572-2.

[12] V. Heera, J. Stoemenos, R. Kögler, M. Voelskow, W. Skorupa, Crystallization and surface erosion of SiC by ion irradiation at elevated temperatures, J. Appl. Phys. 85 (1999) 1378–1386. doi:10.1063/1.369333.

[13] P.O.Å. Persson, L. Hultman, M.S. Janson, A. Hallén, R. Yakimova, D. Panknin, W. Skorupa, On the nature of ion implantation induced dislocation loops in 4H-silicon carbide, J. Appl. Phys. 92 (2002) 2501–2505. doi:10.1063/1.1499749.

[14] V. Heera, R. Kögler, W. Skorupa, J. Stoemenos, Complete recrystallization of amorphous silicon carbide layers by ion irradiation, Appl. Phys. Lett. 67 (1995) 1999–2001. doi:10.1063/1.114766.

[15] A. Heft, E. Wendler, J. Heindl, T. Bachmann, E. Glaser, H.P. Strunk, W. Wesch, Damage production and annealing of ion implanted silicon carbide, Nucl. Instruments Methods Phys. Res. Sect. B Beam Interact. with Mater. Atoms. 113 (1996) 239–243. doi:10.1016/0168-583X(95)01304-0.

[16] Y. Pacaud, J. Stoemenos, G. Brauer, R.A. Yankov, V. Heera, M. Voelskow, R. Kögler, W. Skorupa, Radiation damage and annealing behaviour of Ge+-implanted SiC, Nucl. Instruments Methods Phys. Res. Sect. B Beam Interact. with Mater. Atoms. 120 (1996) 177–180. doi:10.1016/S0168-583X(96)00504-6.

[17] T. Bus, A. van Veen, A. Shiryaev, A.. Fedorov, H. Schut, F.. Tichelaar, J. Sietsma, Thermal recovery of amorphous zones in 6H-SiC and 3C-SiC induced by low fluence 420 keV Xe irradiation, Mater. Sci. Eng. B. 102 (2003) 269–276. doi:10.1016/S0921-5107(02)00712-2.

[18] R. Devanathan, W.. Weber, Displacement energy surface in 3C and 6H SiC, J. Nucl. Mater. 278 (2000) 258–265. doi:10.1016/S0022-3115(99)00266-4.

[19] R.E. Stoller, M.B. Toloczko, G.S. Was, A.G. Certain, S. Dwaraknath, F.A. Garner, On the use of SRIM for computing radiation damage exposure, Nucl. Instruments Methods Phys. Res. Sect. B Beam Interact. with Mater. Atoms. 310 (2013) 75–80. doi:10.1016/J.NIMB.2013.05.008.

[20] S. Sorieul, X. Kerbiriou, J.-M. Costantini, L. Gosmain, G. Calas, C. Trautmann, Optical spectroscopy study of damage induced in 4H-SiC by swift heavy ion irradiation, J. Phys. Condens. Matter. 24 (2012) 125801. doi:10.1002/lary.20355.

[21] J.H. O'Connell, V.A. Skuratov, A.S. Sohatsky, J.H. Neethling, 1.2 MeV/amu Xe ion induced damage recovery in SiC, Nucl. Instruments Methods Phys. Res. Sect. B Beam Interact. with Mater. Atoms. 326 (2014) 337–340. doi:10.1016/J.NIMB.2013.09.034.

[22] S.M. Tunhuma, M. Diale, J.M. Nel, M.J. Madito, T.T. Hlatshwayo, F.D. Auret, Defects in swift heavy ion irradiated n-4H-SiC, Nucl. Instruments Methods Phys. Res. Sect. B Beam Interact. with Mater. Atoms. (2018). doi:10.1016/J.NIMB.2018.11.046.

[23] J.C. Burton, L. Sun, M. Pophristic, S.J. Lukacs, F.H. Long, Z.C. Feng, I.T. Ferguson, Spatial characterization of doped SiC wafers by Raman spectroscopy, J. Appl. Phys. 84 (1998) 6268. doi:10.1063/1.368947.

[24] S. Nakashima, H. Harima, Raman Investigation of SiC Polytypes, Phys. Status Solidi. 162 (1997) 39–64. doi:10.1002/1521-396X(199707)162:1<39::AID-PSSA39>3.0.CO;2-L.

[25] J.C. Burton, F.H. Long, I.T. Ferguson, Resonance enhancement of electronic Raman scattering from nitrogen defect levels in silicon carbide Raman scattering from anisotropic LO-phonon-plasmon-coupled mode in n-type 4H-and 6H, Cit. J. Appl. Phys. 86 (1999) 6268. doi:10.1063/1.371011.

[26] S. Nakashima, T. Kitamura, T. Mitani, H. Okumura, M. Katsuno, N. Ohtani, Raman scattering study of carrier-transport and phonon properties of $4H-SiC$ crystals with graded doping, Phys. Rev. B. 76 (2007) 245208. doi:10.1103/PhysRevB.76.245208.

[27] A. Pérez-Rodríguez, Y. Pacaud, L. Calvo-Barrio, C. Serre, W. Skorupa, J.R. Morante, Analysis of ion beam induced damage and amorphization of 6H-SiC by raman scattering, J. Electron. Mater. 25 (1996) 541–547. doi:10.1007/BF02666633.

[28] R. Héliou, J.. Brebner, S. Roorda, Optical and structural properties of 6H–SiC implanted with silicon as a function of implantation dose and temperature, Nucl. Instruments Methods Phys. Res. Sect. B Beam Interact. with Mater. Atoms. 175–177 (2001) 268–273. doi:10.1016/S0168-583X(00)00633-9.